A strategy for the assembly of three-dimensional mesoscopic structures using a ferrofluid

Ranjan Ganguly, Amit P. Gaind, and Ishwar K. Puri

Citation: Physics of Fluids (1994-present) **17**, 057103 (2005); doi: 10.1063/1.1899695
View online: http://dx.doi.org/10.1063/1.1899695
View Table of Contents: http://scitation.aip.org/content/aip/journal/pof2/17/5?ver=pdfcov
Published by the AIP Publishing

PHYSICS OF FLUIDS **17**, 057103 (2005)

A strategy for the assembly of three-dimensional mesoscopic structures using a ferrofluid

Ranjan Ganguly[a] and Amit P. Gaind
Mechanical and Industrial Engineering Department, University of Illinois at Chicago, Chicago, Illinois 60607

Ishwar K. Puri[b]
Department of Engineering Science and Mechanics, Virginia Polytechnic Institute and State University, Blacksburg, Virginia 24061

(Received 21 August 2004; accepted 11 March 2005; published online 26 April 2005)

A novel technique for the self-assembly of three-dimensional mesoscopic structures in a forced fluid flow by employing a magnetic field is described. There are advantages of using magnetic fields for this purpose: unlike many other forces, a magnetic force is effective even from a distance, permitting "action at a distance," it is also localized, and competition between the magnetic force and fluid shear enables unique self-assembled ferrofluid structures. Herein, a simulation provides insight into the possibility of using magnetic field to assemble colloidal nanoparticles into aggregates. Subsequently, a demonstration experiment is conducted to characterize the development and decay of such aggregates. The analysis provides a basis for developing effective self-assembly techniques for various engineering applications. © *2005 American Institute of Physics*.
[DOI: 10.1063/1.1899695]

I. INTRODUCTION

A self-assembly process is characterized by the spontaneous and ordered aggregation of similar components. At the nanoscale, these constituents can be colloids, or other nanoparticles that combine to form structures of mesoscopic and macroscopic dimensions. Self-assembly is most evident during the growth of biological structures. Due to its natural elegance, there is considerable interest in investigating similar methods in the physical and chemical sciences. At the supramolecular level, dynamic self-assembly can be used to prepare adaptive materials[1] for photonic[2] and MEMS (microelectromechanical systems) devices.[3] This is characterized by a competition between at least two forces—one attractive and the other repulsive—in systems that are not in thermodynamic equilibrium, and it is associated with energy dissipation. Several researchers have described self-assembly in configurations where biological[4] or chemical[5] mediation, electrostatic,[6] capillary,[7] or fluid dynamic[8,9] forces have provided a motive potential.

The self-assembly of ferromagnetic nanoparticles is a promising technique for producing high density magnetic data storage devices[10] and three-dimensional memory chips.[11] Ferrofluids are colloidal suspensions of single domain magnetic nanoparticles that are typically of the order of 10 nm in diameter. At room temperature the thermal Brownian energy of the individual particle magnetic domains supercedes the magnetocrystalline anisotropy energy and the nanoparticles exhibit superparamagnetic behavior,[12] since for ferrous nanoparticles of this size, the blocking temperature[13] is much lower than the room temperature. In this case, unlike the behavior of bulk material, the particle magnetization does not exhibit hysteresis. In the absence of an external magnetic field, the individual particle dipoles are randomly oriented due to thermal agitation. Consequently, the fluid does not show any permanent magnetization. However, the fluid bulk starts to exhibit magnetic behavior when an imposed magnetic field induces the alignment of the thermally disoriented magnetic moments of these particles.

The nanoparticles are coated with adsorbed surfactant layers to prevent particle agglomeration due to the van der Waals forces and dipole-dipole interactions among them. The presence of the surfactant helps maintain an adequate spacing between the particles so that the attraction energy between adjacent particles is smaller than the disordering energy of their thermal motion, thereby providing colloidal stability. Consequently, a ferrofluid can often be considered as a single homogeneous liquid.[14,15] Such fluids can be collected into homogeneous aggregates by applying external magnetic fields.[15,16]

Ferrofluids have been used to form patterns on flat substrates.[17,18] For instance, a thin ferromagnetic film can be patterned into isolated islands and used to direct the assembly of superparamagnetic colloidal particles into two-dimensional arrays.[19] However, previous research has focused on the self-assembly of two-dimensional patterns rather than of complex three-dimensional architectures. When a sessile drop of ferrofluid placed on a flat substrate is subjected to a spatially varying magnetic field, the interactions between gravity, surface tension, and the magnetic force create different shapes.[20]

We have been able to create three-dimensional mesoscopic ferrofluid structures and arrays of various configurations on flat substrates.[21] Figure 1(a) presents an image of a

[a]Also at Power Engineering Department, Jadavpur University, Kolkata 700032, India.
[b]Author to whom correspondence should be addressed. Electronic mail: ikpuri@vt.edu

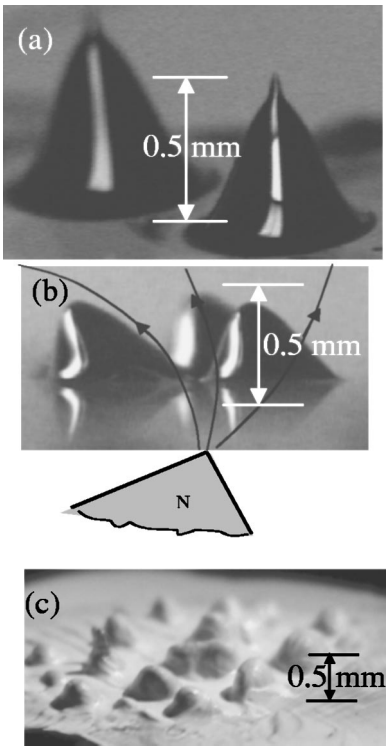

FIG. 1. (a) Three-dimensional ferrofluid structures produced on a flat substrate using a bar magnet, (b) varying orientations of these structures with respect to the magnetic lines of force, and (c) permanent ferrofluid structures made by mixing a curing agent with the ferrofluid and then curing under a magnetic field.

mesoscale three-dimensional (3D) structure produced by a hydrocarbon oil-based EFH 1 ferrofluid (FerroTec USA, NH) that was placed on a wetting glass surface under the influence of the nonuniform magnetic field. The height, shape, and orientation of such microliter droplets can be adjusted by altering the nature of the magnetic field, as shown in Fig. 1(b). Although such aggregates are semipermanent in nature (i.e., they go away when the magnetic field is withdrawn) permanent structures have also been created in our laboratory by mixing a ferrofluid with a fast cure silicone elastomer (Sylgard® 170) and curing the resulting droplets while they are under prolonged exposure to a magnetic field [refer to Fig. 1(c)].

Several ferrofluid applications, e.g., microfabrication, ferrofluid-based switches, and valves or magnetic drug delivery, can benefit from the self-assembly of magnetic nanoparticles in flows that are characterized by advection. A ferrofluid can be mixed with wet etching chemicals and introduced into narrow channels (where masking is otherwise difficult). Thereafter, it can be deposited on the substrate wall locally and selectively by imposing a suitably designed magnetic field. Thus, maskless etching of microscale or mesoscale channels can be achieved using targeted ferrofluid aggregation.

Three-dimensional ferrofluid aggregates can also be used as microfluidic components in pumps and valves[22] or as microsize contact switches. In a ferrofluid micropump, a magnetic field-driven ferrofluid droplet acts as a reciprocating piston in a microchannel to pump another fluid. In microvalves, ferrofluid aggregates (formed by imposing a magnetic field) are used to open or close the flow in a microchannel. In ferrofluid microcontact switches, liquid bridges of electrically conductive ferrofluids are formed under the influence of a magnetic field to establish contacts between two electrodes that are immersed in an immiscible fluid. All these microfluidic applications rely on the phenomenon of ferrofluid aggregation under an imposed magnetic field. For these devices to work, it is important that the ferrofluid structures maintain their integrity against the shear force exerted by another fluid flow over them.

Another application, magnetic drug delivery,[23] requires that a given volume of drug-laden ferrofluid droplet be delivered in the form of an aggregate at a target location *in vivo* through the blood vessel or lymphatic system where it is localized until the medicinal drug disperses from the ferrofluid droplet into the affected area. Here, the challenge is to hold the ferrofluid aggregate in position against the blood (or lymphatic) flow in a vessel next to the target location. In order to investigate the efficacy of the drug targeting, the drug desorption in the target area must be investigated. Firsthand information on this can be achieved by analyzing the ferrofluid aggregate size that is localized at the target area and its dispersion under the shear force induced by blood (or lymphatic) flow.

The literature contains very little work related to characterizing the fluid dynamics of ferrofluid aggregate formation,[24] which has motivated the current investigation. The goal of the present work is to propose novel ferrofluid self-assembly scenarios through which three-dimensional structures can be produced by a balance between the magnetic body force and the fluid shear. The formation of these structures in forced flows is described herein and the relevant transport is characterized.

First, numerical simulations are conducted in a representative two-dimensional configuration to obtain fundamental understanding about the formation of tangible ferrofluid structures in forced flows under the influence of a magnetic field. The flow and nanoparticle concentrations around the self-assembled structures are analyzed to identify the interactions between the various forces that influence ferrofluid accumulation and dispersion. Next, experiments are performed to demonstrate the formation and subsequent decay of 3D mesoscopic ferrofluid structures in a steady pipe flow of a miscible host fluid. In the experiments, a ferrofluid structure dynamically self-assembles near a magnetic dipole during an initial phase when a specified amount of ferrofluid is injected. Thereafter, ferrofluid injection ceases and the process variables (i.e., the water flow rate and the magnetic field) are held unchanged to observe the disintegration of the structures. The overall process involving the buildup of this structure and its subsequent dissolution is in nonequilibrium.

Permanent structures can be created by mixing low-viscosity epoxy resins with the ferrofluid, applying a magnetic field to create ferrofluid structures and curing them. Since the final size and shape of a hardened structure will depend upon that of an aggregate at the instant of curing (provided that the curing time is significantly smaller than the dispersion time scale), it is important that we are able to

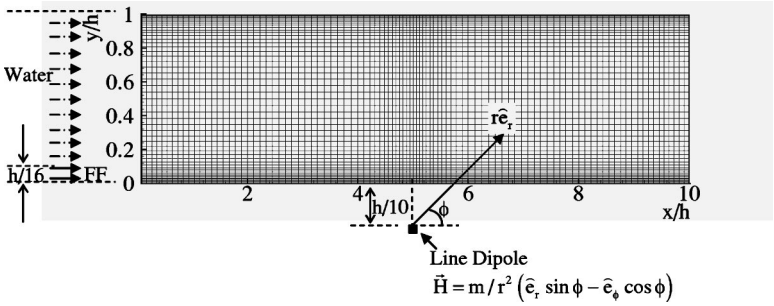

FIG. 2. Schematic of the computational domain.

characterize both the initial growth and the subsequent decay of a structure created with a specified amount of ferrofluid.

II. SIMULATIONS

The ferrofluid is injected into a forced flow that is established with a nonmagnetic host fluid upstream of a location where a magnet is placed. Ferrofluid transport first occurs from the point of injection through advection. Near the magnet, the magnetic body force dominates the advective-diffusive ferrofluid transport and leads to its local buildup. A two-dimensional channel flow is simulated in order to obtain insight into the ferrofluid transport and the competition between the magnetic and viscous forces during the formation of the localized self-assembled structures. Figure 2 contains a schematic diagram of the computational domain. The ferrofluid is allowed to enter through a narrow section at the inlet adjacent to the lower wall. A line dipole is placed near the lower wall half way along the channel length, which provides a two-dimensional magnetic field, as described elsewhere.[25,26]

The nanoparticle concentration in the ferrofluid is considered small enough for the dipole-dipole interactions to be negligible (since the largest volume fraction of the particles is 3%). Therefore, Langevin's theory[27] can describe the fluid magnetization sufficiently accurately.[28] As described by Berkovsky,[12] each of the nanoparticles of ferrofluid possesses a definite magnetocrystalline anisotropy energy component (which is a function of the particle size, shape, and crystallographic structure) and thermal Brownian energy component (that is a function of the temperature). While the first component is responsible for the rotation of a magnetic particle (that has a definite particle moment) to align it with an imposed magnetic field, the latter one produces random thermal fluctuations of the magnetic moment within the particle. Here, we have considered a fluid type for which the total magnetocrystalline anisotropy energy of the nanoparticles is much lower than their thermal fluctuation energy. This implies that the magnetic moment of a domain is not rigidly fixed to the particle body. Therefore, the magnetic field does not influence the particle orientation. The magnetoviscous effect (which is the change of effective fluid viscosity due to the forced alignment of particles in the direction of imposed magnetic field) and consequent anisotropies in other fluid properties are hence negligible.[29] Also, since the magnetic moments are not "frozen" inside the particles, the particle rotation (that occurs in a rotational flow field) does not alter the orientation of the individual particle magnetic moment (which tends to align itself with the imposed field). Thus, the viscous torque on the nanoparticles does not have to overcome the magnetic torque so that the fluid is free from magnetodissipation.[30]

The magnetic field **B** and the variable **H** [$=(\mathbf{B}/\mu_0 - \mathbf{M})$, where μ_0 denotes the permeability of vacuum and **M** the magnetization of the medium] obey the Maxwell's equations in static form,[31] i.e.,

$$\varepsilon_{ijk}\,\partial H_k/\partial x_j = 0 \quad \text{(no free current)}, \tag{1}$$

$$\partial B_j/\partial x_j = 0. \tag{2}$$

The mass, momentum, and species equations solved to obtain the velocity **v**, pressure p, and the mass fraction of nanoparticles in the host fluid, Y_f fields are

$$\partial\rho/\partial t + \partial(\rho v_j)/\partial x_j = 0, \tag{3}$$

$$\partial(\rho v_i)/\partial t + \partial(\rho v_j v_i)/\partial x_j = -\,\partial p/\partial x_i + \partial\tau_{ij}/\partial x_j + \Im_i, \tag{4}$$

$$\partial(\rho Y_f)/\partial t + \partial[\rho v_j Y_f - \rho D\,\partial Y_f/\partial x_j + 1/(6\pi\eta a)\rho Y_f f_j]/\partial x_j = 0. \tag{5}$$

The viscous stress tensor τ_{ij} that appears in the momentum equation is expressed in terms of the fluid viscosity η and velocity gradient as

$$\tau_{ij} = \eta(\partial v_i/\partial x_j + \partial v_j/\partial x_i) - (2/3)\,\eta\delta_{ij}(\partial v_k/\partial x_k), \tag{6}$$

where δ_{ij} denotes the Kronecker delta. The last term in the momentum equation contains the Kelvin body force expressed per unit volume $\Im_i = M_j(\partial B_j/\partial x_i)$ (Ref. 32) that arises from the fluid magnetization (due to the presence of the magnetic nanoparticles) in the imposed magnetic field. The magnetization of the fluid is obtained from Langevin's formula, i.e., $M = \varphi M^{\text{sat}}\{\coth(\alpha) - (1/\alpha)\}$, where φ is the volume fraction of magnetic particles in the fluid, M^{sat} the bulk saturation magnetization of the particle material and $\alpha = \mu_0 m^p H/kT$ is the Langevin parameter. Here, m^p denotes the magnitude of dipole moment of a single particle [$=4/3\pi a^3 M^p$, for a particle magnetization $M^p = M^{\text{sat}}\{\coth(\alpha) - (1/\alpha)\}$], T denotes the absolute temperature and k the Boltzmann constant. Since we consider a dilute ferrofluid, the diffusivity of the magnetic nanoparticles (having radius a) can be obtained using the Stokes–Einstein equation,[33] i.e.,

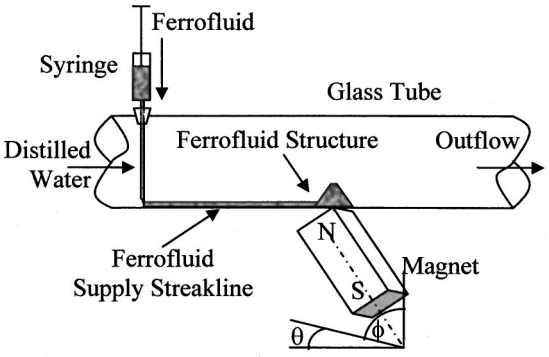

FIG. 3. Schematic diagram of the experimental setup.

$$D = kT/6\pi\eta a. \tag{7}$$

The last term in the species equation represents magnetophoretic motion, which arises due to Stokesian migration of superparamagnetic nanoparticles under the magnetic force $f_j = \mu_0 m^p{}_k \partial H_j/\partial x_k$.[32] Here, m_k^p denotes the component of the particle moment vector along x_k axis. The local fluid density ρ is related to the local volumetric mass fraction of the nanoparticles through the expression,

$$\rho = (\rho^p - \rho^l)\varphi + \rho^l, \tag{8}$$

where ρ^p and ρ^l denote the densities of the particles and the host liquid, respectively. The volume fraction of the particles is related to their mass fraction through the expression,

$$\varphi = \rho^l Y_f/[\rho^p - (\rho^p - \rho^l)Y_f]. \tag{9}$$

The coupled equations (3)–(5) are solved using the SOLA (Solution Algorithm) explicit finite-difference numerical technique.[34] The variables ($\mathbf{v}, p$, and Y_f) and the fluid properties are described on a staggered grid. The axial and transverse velocities are specified at the cell faces while the pressure, temperature, and the fluid properties are stipulated at the cell centers. The advection terms are discretized through hybrid differencing and the diffusion terms by central differencing to avoid numerical diffusion.[35] Successive solutions are obtained using time marching. The variable grid, which is required to resolve the sharp gradients near the walls and close to the location of the magnetic dipole and the magnetic fluid structures, is based on a hyperbolic mesh size distribution. A 70×50 mesh is found to provide the best grid-independent results.

III. EXPERIMENT

Figure 3 contains a schematic diagram of our experimental setup in which the three-dimensional ferrofluid structures are built. In the experiments, a known volume of EMG 705-series (FerroTec USA, NH) water soluble ferrofluid is released from a microliter syringe pump into a steady laminar pipe flow of distilled water through a horizontally mounted glass tube. The tube internal diameter is 10 mm and the test section is 1 m long. The syringe needle enters the tube vertically through a rubber plug and reaches the bottom of the tube, as shown in the figure. An AlNiCo 5.7 [a high quality magnetic material having ⟨100⟩ crystal structure and cast by adding cobalt to ternary alloys of Al, Ni, and Fe (Ref. 36)] permanent magnet ($2.54\times 2.54\times 6$ cm^3) of 1.3 T residual magnetism (0.5 T at pole face) is placed under the tube 100 mm downstream of the injection location to create the magnetic field. The position and angular orientation of the magnet can be altered since it is mounted on a graduated arc slider with two degrees of rotation and is also capable of moving in a direction perpendicular to the tube. The dispersion and localization of the ferrofluid are observed from direct images. These are acquired using a charge-coupled device camera against a white backlight (since the ferrofluid is dark and opaque). The flow Reynolds number Re is adjusted by precise control of the water flow rate.

IV. RESULTS AND DISCUSSION

A. Simulation results

The numerical simulation is performed in a steady, forced flow for a Reynolds number Re=250. Distilled water (with a density $\rho^l = 1000$ Kg/m^3 and viscosity $\eta = 0.001$ Pa s) is chosen as the host fluid and the Re value is based on the host fluid inlet velocity, channel height, and the host fluid properties. The ferrofluid, having a particle density $\rho^p = 5240$ Kg/m^3 and volume fraction $\varphi_{\text{in}} = 0.03$, is injected steadily at the inlet between the planes $y/h = 0$ and $1/16$. A plug velocity profile is assumed at the inlet, implying that the ferrofluid and the host fluid have the same velocity there. For an average particle diameter of ~10 nm, the ferrofluid diffusivity (as per the Stokes approximation) in distilled water is of the order of 10^{-11} m^2/s.[37] Hence, very little diffusive dispersion of the ferrofluid occurs in the cross-stream direction and its transport closely follows the streamlines of the developing flow. In the absence of a magnetic field (for zero dipole strength), the ferrofluid would be transported downstream in the Poiseuille flow and exits the computational domain within the corresponding advection time scale. There would have been little transverse diffusion of ferrofluid. However, as the dipole strength is increased, the magnetic body force alters the flow field in regions where both the magnetic field gradient and the ferrofluid concentration are large. Figures 4(a) and 4(b) present the velocity vectors and the normalized ferrofluid particle volume fraction contours $\Phi^*(=\varphi/\varphi_{\text{in}})$ for two different magnetic dipole strengths, i.e., $m = 0.1$ and 0.5 A m, respectively. Both the plots are obtained after the steady state is reached (i.e., when the field variables do not change with time anymore). Because of the magnetic body force, the ferrofluid collects near the line dipole and builds a local structure in the form of a region of high concentration. At the same time, advective-diffusive transport of the nanoparticles takes place from this region to downstream locations. The aggregate initially grows as the ferrofluid supply from the inlet exceeds its washaway rate. However, after it reaches a critical size, the ferrofluid dispersion rate is equal to its influx and stable structures, as described in Figs. 4(a) and 4(b), are established.

In order to explain the nanoparticle assembly, the Kelvin body force $\mathfrak{J}_i$ on the fluid must be analyzed. It is a function of local magnetic field B_i and the local magnetic susceptibility $\chi_m = M/H$ of the medium, i.e.,

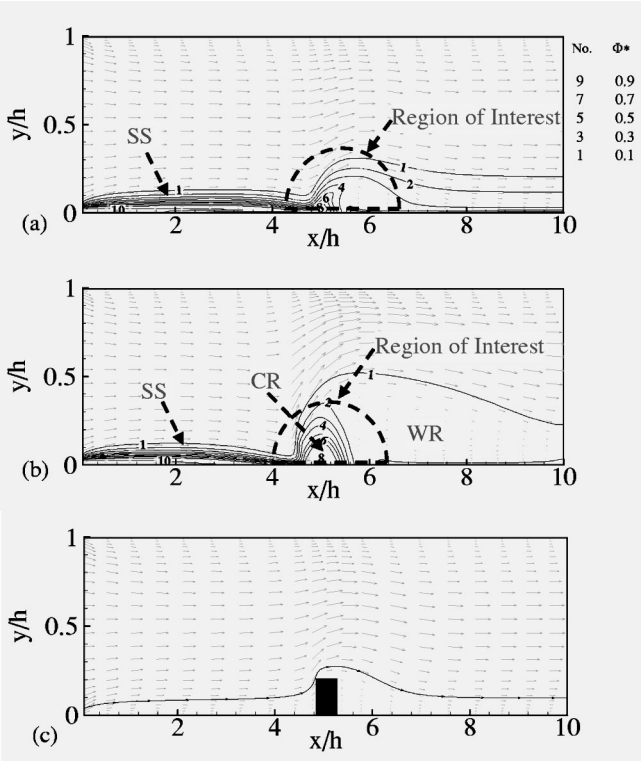

FIG. 4. Steady-state ferrofluid structures represented by the normalized particle volume fraction Φ^* contours ($=\varphi/\varphi_{in}$). The structures are formed due to the influence of a line dipole with strengths of (a) 0.1 A m and (b) 0.5 A m. Ferrofluid dispersion from the structures due to hydrodynamic shear is steadily replenished through a continuous supply from the inlet. Arrows indicate the velocity vectors. (SS=supply streaklines, CR=core region, WR=washaway region.) (c) Recirculation profile [almost identical to that in (a)] produced by a solid obstacle of normalized length×height=0.45×0.2 placed in a Poiseuille flow of same Reynolds number.

$$\mathfrak{J}_i = \mu_0\chi_m(1+\chi_m)\,\partial(H^2/2)/\partial x_i + \mu_0\chi_m H^2\,\partial\chi_m/\partial x_i. \quad (10)$$

The first term in the Kelvin body force produces a magnetostatic pressure that has a linear dependence on the gradient of H^2. For the line dipole, the isobars form cylindrical contours around its virtual origin. Thus, when the magnetostatic pressure is large [as in the case corresponding to Fig. 4(b) when $m=0.5$ A m], the ferrofluid aggregate produced near the line dipole assumes a cylindrical shape. We refer to this as the "core" region [Fig. 4(b)].

The magnetostatic pressure decreases rapidly moving away from the dipole, since it is proportional to the ratio $1/r^5$. Consequently, the second term in Eq. (10) that arises due to the spatial gradient in the particle density becomes larger than the preceding term. However, its value also decreases significantly at locations further away from the dipole. Therefore, the particle concentration contours in regions relatively removed from the dipole are not cylindrical. Instead, they are shaped by the advective-diffusive nanoparticle transport in the flow field. This is referred to as the "washaway" region [Fig. 4(b)]. This process also occurs for relatively small dipole strengths, e.g., the ferrofluid concentration contours for a dipole strength $m=0.1$ A m [see Fig. 4(a)]. Here, the core region is not well developed. On the contrary, when $m=0.5$ A m the aggregate core is clearly visible. If we track the $\Phi^*=0.5$ contour as being representative of the core region size, the core height increases 1.5 times when the dipole strength increases fivefold (from 0.1 A m to 0.5 A m). In this case, the magnetic body force is on an average 25 times stronger, since $\mathfrak{J}$ is linearly dependent on M and B, and for small values of m, M and B are proportional to m.

Figures 4(a) and 4(b) show that there is a departure from the Poiseuille flow profile, since the streamlines move away from the lower wall at upstream locations before the aggregate. However, the ferrofluid continues to move along the lower wall towards the dipole, since it is pulled in the direction of increasing magnetic field strength. The velocity vectors in Figs. 4(a) and 4(b) show that boundary layer separation and flow recirculation occur downstream of the ferrofluid aggregate. A large magnetostatic pressure near the dipole induces flow stagnation in a manner similar to that produced by a solid obstacle placed in a flow. Figure 4(c) compares the flows induced by the ferrofluid aggregate at $m=0.1$ A m [Fig. 4(a)] and a solid obstacle of normalized length×height=0.45×0.2 placed on the channel wall with the two flows at identical Reynolds numbers. The ferrofluid dispersing into the flow from the core collects temporarily in this recirculation region and creates the washaway region. Likewise, in Fig. 4(c), the streamline adjacent to the solid obstacle is in qualitative agreement with the shape of the washaway region downstream of the ferrofluid aggregate.

B. Experimental results

The simulation presented in the preceding section predicted two-dimensional free-standing structures and provided insight into how a ferrofluid could be accumulated in a forced flow. We have conducted a proof-of-concept experiment in a steady cylindrical pipe flow. Here, the flow in the vicinity of the high magnetic field gradient produces a dynamic interaction between the fluid shear and magnetic body force and produces three-dimensional structures. In the experiment, ferrofluid is injected at a rate of ~ 1 μl/s into a steady, fully developed pipe flow established at Re=250. There is no further ferrofluid injection into the flow after 3 μl of ferrofluid is introduced, but the host fluid flow is maintained at the same value. The ferrofluid has a higher density than water and, as mentioned earlier, undergoes very little cross-stream dispersion due to its relatively small diffusivity. Consequently, after leaving the injector tip, the ferrofluid is advected downstream in the form of a narrow streakline along the lowermost section of the tube (Fig. 2). This is similar to the simulation results. Likewise, as in the simulations, the magnetic body force alters the flowfield in the vicinity of the dipole during the experiment.

When the bar magnet is held at an angle $\theta=\phi=45°$ (cf. Fig. 2) with a corner touching the outer wall of the tube, the ferrofluid forms a conical structure due to the action of the magnetic body force. Figure 5(a) presents the time evolution of ferrofluid accumulation near the magnet after the entire 3 μl of the ferrofluid has been introduced. The entire ferrofluid mass is transported by advection to the region near the dipole tip in 100 s [streaklines for which are visible in

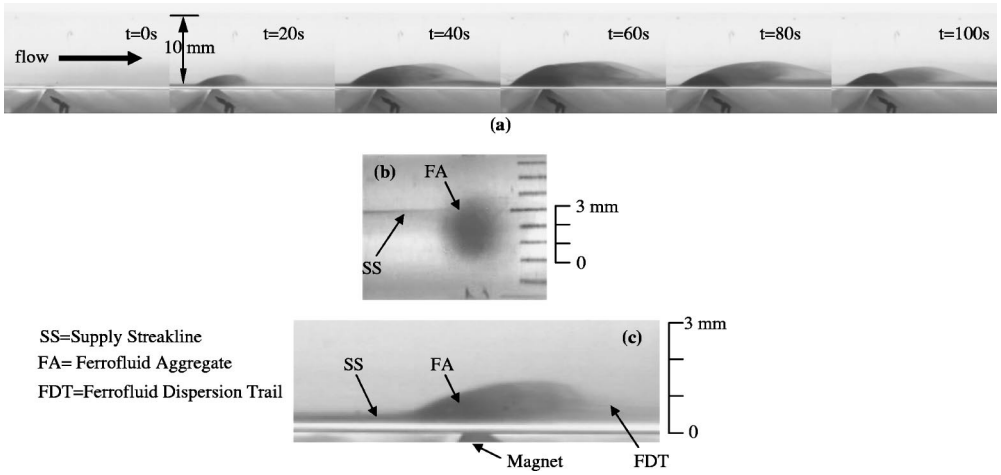

FIG. 5. Experimental evidence of aggregation of the ferrofluid due to the competition between the magnetic body force and the coupled advective-diffusive dispersion. (a) Time evolution of the accumulation phase ($t=0-100$ s after injection, which also includes the first washaway cycle). (b) Top view and (c) front view of the aggregate at $t=20$ s show streaklines, which provide the advected ferrofluid supply from the injection location. The front view also shows evidence of dispersion from the ferrofluid aggregate. The volume of injected ferrofluid is 3 μl and the flow Re=250.

Figs. 5(b) and 5(c)]. The ferrofluid accumulation rate exceeds its washaway rate during this time and the size of the nanoparticle aggregate grows into a conical shape [as shown by the sequence of images in Fig. 5(a)]. Once fresh supply to the aggregate ceases, the advective and diffusive transport of the ferrofluid into the continually flowing host water stream leads to a depletion in the nanoparticle cluster. This phase is presented through the image sequences in Figs. 6(a) and 6(b).

Figure 6(c) presents an enlarged image of the accumulated structure at $t=240$ s. The existence of a dark core region provides evidence of higher ferrofluid concentration close to the dipole. The image on the right [Fig. 6(c)] is contrast enhanced in order to better illustrate the recirculation. The movie image sequence indicates that the recirculation is clockwise.

C. Discussion

Both the numerical simulation and the experiment were performed in steady host flows, but there are some differences. Since a steady supply of ferrofluid is maintained in the simulations, the predicted dispersion also pertains to steady state (after an initial transient ceases). In contrast, the experimentally observed dispersion is unsteady (since further ferrofluid supply ceases after 3 μl are injected). The simulation is performed in a two-dimensional rectangular channel, while the experiment is performed in a cylindrical geometry. Consequently, the simulated ferrofluid aggregate has a different geometric attribute (prism shaped with a nearly triangular cross section and large third dimension) while the experiment produces a conical shape. Nonetheless, the simulation provides useful qualitative information regarding the forma-

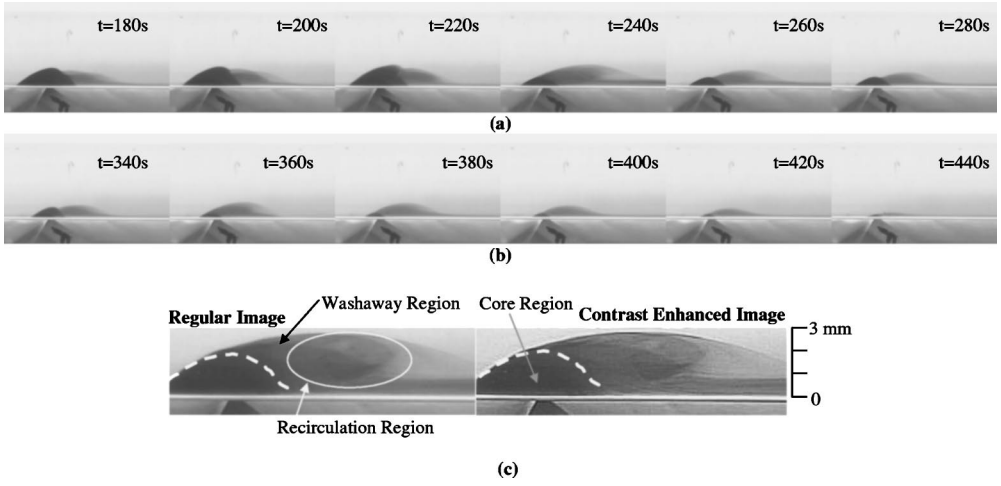

FIG. 6. Time evolution during the depletion phase of the ferrofluid structure (the volume of injected ferrofluid is 3 μl and the flow Re=250): (a) $t=180-280$ s during the second washaway cycle and (b) $t=340-440$ s during the third washaway cycle. (c) Ferrofluid structure at $t=240$ s after injection. The combined advective-diffusive hydrodynamic force competes with the magnetic force to produce a tightly bound core region that is immediately followed by a downstream washaway region. The contrast enhanced image in the right is provided for better visualization of the flow recirculation.

tion of a ferrofluid aggregate and its dispersion, and, therefore, can be used to explain the experimentally observed phenomena.

Both the simulations and experiments show that the core behaves as a solid obstruction in the flow and creates downstream recirculation. Here, the magnetic body force on the nanoparticles exceeds the shear force applied by the host fluid flow and causes them to move closer to the dipole. This further increases the magnetic force that they experience, pushing them more inward. Thus, a tightly bound core region is formed. The front view of this aggregate in Fig. 6(c) strongly resembles the simulated core region presented in Fig. 4(b). An outward ferrofluid flux occurs due to the presence of a large local concentration gradient at the periphery of this core [Fig. 4(b) presents the comparable simulation results]. As the particles travel outward from the core through diffusion, the magnetic force on them weakens. Hence, the shear force exerted by the main flow becomes comparable to the restoring magnetic force. Consequently, ferrofluid dispersion occurs from the boundary demarcating the core. As the core boundary erodes, ferrofluid recirculates in this wake or washaway region. In this region, the magnetic body force is much weaker than in the core because of the smaller ferrofluid concentration and larger displacement from the dipole. Hence, ferrofluid is readily transported away from the washaway region through the influence of the host flow. This is clearly observed both in Figs. 4(a) and 4(b) (from the velocity vectors) and Fig. 6(c).

Depending upon the application, the flow recirculation occurring in the washaway region can have favorable or detrimental effects. For example, in ferrofluid microvalves or pumps, the recirculation is undesirable, since it leads to additional channel pressure loss. On the contrary, in micromixing devices, ferrofluid structures can be constructed to achieve additional recirculation and enhance the cross-stream mixing (which is generally extremely slow in microchannels). In magnetic drug targeting applications, the creation of the washaway region due to the flow recirculation is favorable, since it allows the ferrofluid (and the medicinal drug functionalized with it) to stay longer in the vicinity of the target organ.

Erosion of the ferrofluid aggregate occurs in cycles, i.e., the projected areas of the core and the washaway region in particular are observed to first increase with time [for example, the washaway region is observed to swell from $t=180$ s to $t=240$ s in Fig. 6(a)]. Then, a substantial amount of ferrofluid is suddenly washed away downstream. This is accompanied by a rapid shrinking of the aggregate size [as seen in Fig. 6(a) where the washaway region shrinks quickly between $t=240$ and 260 s]. We refer to this behavior as the washaway cycle. Since there is continuous loss of ferrofluid from the aggregate, its final size after each washaway cycle is progressively smaller. Figures 6(a) and 6(b) show this behavior for two consecutive cycles.

We have analyzed the front view image sequence [of which images in Figs. 5(a), 6(a), and 6(b) are only a selected few and represent three different periods during the same experiment] based on the local pixel intensity (i.e., the relative local darkness of the fluid), and determined the time evolution of the projected area of the core and washaway regions during $t=0-600$ s in Fig. 7. Four distinct washaway cycles are observed for the accumulated 3 μl ferrofluid volume during the experiment. These are marked as *C*-I–*C*-IV in Fig. 7. For ease of comparison, images of the "peaks" and "troughs" in the aggregate size are also superposed on Fig. 7. These images correspond to $t=80$ s (first washaway region size peak), 100 s (supply of injected ferrofluid to the aggregate stops), 160 s (first peak in core size after the injection ceases and it coincides with the first trough in washaway region size), 220 s (second washaway region size peak), 260 s (second core region size peak), 300 s (washaway region size trough), 350 s (washaway region size peak), 450 s (washaway region size trough), and 520 s (washaway region size peak). Careful observation of Fig. 8 indicates that the erosion of the core precedes ferrofluid dispersion from the washaway region in each washaway cycle.

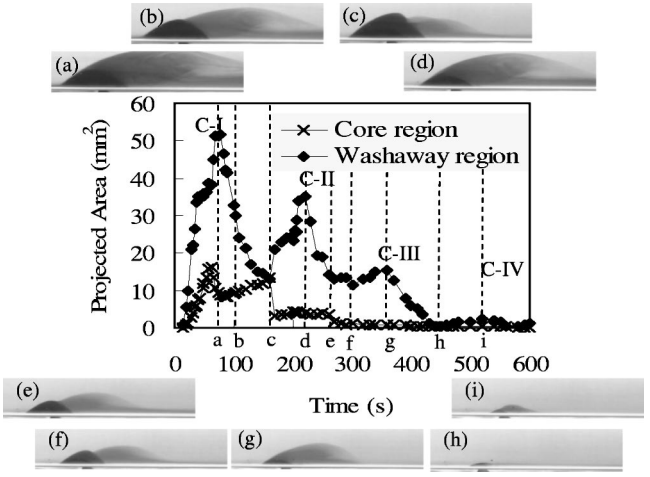

FIG. 7. Time evolution of the projected front view area of the core and washaway regions. Four washaway cycles (*C*-I–*C*-IV) are observed from the experiment. Images (a) through (i) represents the "crests" and "troughs" for the projected apparent area of the core and washaway regions.

Although the ferrofluid aggregate is continuously losing nanoparticles with the flow and is not replenished by fresh supply, the projected area of the core and washaway regions are found to wax and wane with time (using the image pixel information). Figure 8 shows a sequence of schematic diagrams of the washaway cycle to suggest a plausible explanation of this anomalous behavior. The core region has high particle loading so that the pixels record no light signal. Hence, it appears uniformly dark [refer to Fig. 8(a)]. When the particles from the core region diffuse outward because of concentration gradient, the particle concentration in the peripheral region of the core remains large enough to maintain the darkness. Thus, optically, the core appears to distend slightly [refer to Fig. 8(b)]. This is also observed in Fig. 7, where the core appears to grow from image (b) ($t=100$ s) to image (c) ($t=160$ s). This is an artifact, since the particle concentration of the periphery of the distended core should decrease due to mass conservation arguments.

As the core expands and the ferrofluid density decreases, the fluid shear force at its boundary becomes comparable to the magnetic force (since the magnetic force per unit volume

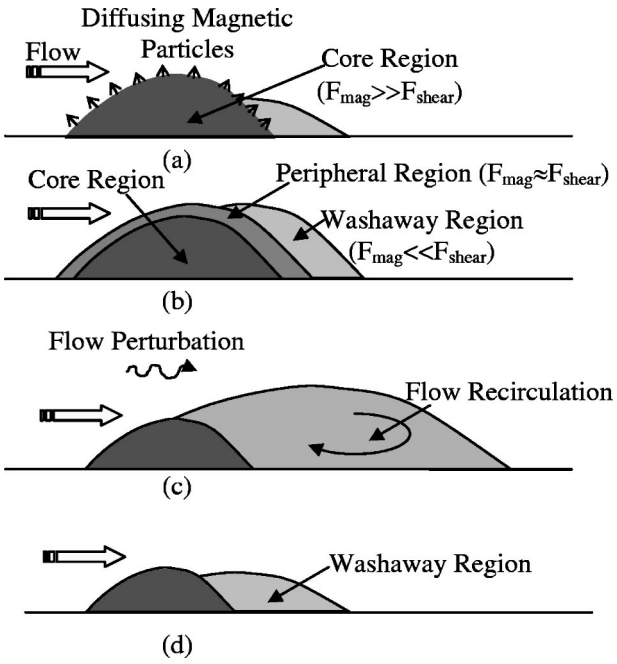

FIG. 8. Schematic diagram showing the phases of the ferrofluid washaway that lead to apparent oscillations of the core and washaway regions during one washaway cycle: (a) Diffusion of ferrofluid from core, (b) core region apparently swells in size creating a loosely bound peripheral region, (c) flow perturbation dislodges the ferrofluid from the peripheral region and the particles collect in a recirculating washaway region—washaway region that suddenly grows in size, (d) washaway region gradually depletes due to downstream advective transport of the ferrofluid.

is proportional to the local particle concentration). Flow perturbations during the experiment create vortex shedding[38] in the wake of the ferrofluid structure. The balance of the magnetic and shear force in the peripheral region is unstable because even slight dislocation of a particle away from the core by shear causes the magnetic force to diminish. In that case, small perturbations lead to sudden ferrofluid release from the core periphery. These dislodged particles form a large washaway region in the wake [refer to Fig. 8(c)]. As the host flow continues to transport the particles downstream, the size of the washaway region shrinks [as shown in Fig. 8(d)], until another ferrofluid mass is shed from the core.

The time associated with a single washaway cycle is roughly 100 s. Since the overall host fluid velocity is ~ 1 cm/s [$u \sim \mathrm{Re}\,\eta/(\rho^l \times$ pipe diameter)] and the characteristic aggregate dimension ~ 1 cm, the advection time is ~ 1 s, which, being two orders of magnitude smaller, is a poor indicator of the washaway cycle time. However, the viscous time scale [i.e., (aggregate height)^2/kinematic viscosity], which is also ~ 100 s, provides a better correlation. That the process is not diffusion dominated is affirmed by comparing the washaway time with the relatively long diffusion time. Considering a ferrofluid mass diffusivity of $\sim 10^{-11}$ m^2/s,[37] the diffusion time [that approximately equals the (aggregate height)^2/particle diffusivity] is $\sim 10^7$ s or five orders of magnitude larger than the washaway time. The similarity between the viscous and washaway cycle times indicates that viscous shear of the ferrofluid aggregate plays a major role during the washaway process.

The image sequences in Figs. 6(a) and 6(b) and the curves presented in Fig. 7 illustrate the devolution of the core and the washaway regions over time. The washaway cycles play an important part in determining the instantaneous size of the aggregate. They also provide important information related to the curing time required for any binding agent to solidify in order to establish more enduring three-dimensional structures. While the analysis presents two types of possible structures through the simulation and the experiment, a larger variety of structures[21] can be built through arrays and combinations of these geometries.

V. CONCLUSIONS

The formation of three-dimensional mesoscopic structures using a ferrofluid injected into a forced water flow is first simulated and then experimentally examined.

(A) The simulation predicts the formation of aggregates for a steady ferrofluid supply in a two-dimensional flow. The shapes and sizes of the structures depend on the nature of the imposed magnetic field. A more distinct core region is observed for higher dipole strengths. When the dipole strength is high, the magnetostatic pressure generated in the ferrofluid produces flow stagnation.

(B) An experiment is performed to demonstrate the formation of ferrofluid aggregates in a steady pipe flow. When a finite ferrofluid volume is injected into the system, two phases are observed. Initially, the ferrofluid supply exceeds its dispersion into the host flow so that a conical structure grows near the dipole. During the second phase after the fresh supply of ferrofluid ceases, the structure diminishes over time due to ferrofluid dispersion.

(C) The experimentally observed structure consists of a tightly bound core where the ferrofluid concentration is high. The core region behaves analogous to a solid obstacle placed in the flow and creates a flow recirculation in its wake. Ferrofluid dispersed from the core region collects in this recirculating region, giving rise to a loosely bound washaway region. The core and washaway regions show periodic swelling and shrinkage with a gradual overall depletion in size.

[1] P. Alstrom and D. Stassinopoulos, "Versatility and adaptive performance," Phys. Rev. E **51**, 5027 (1995).
[2] E. W. Seeling, B. Tang, A. Yamilov, H. Cao, and R. P. H. Chang, "Self-assembled 3D photonic crystals from ZnO colloidal spheres," Mater. Chem. Phys. **80**, 257 (2003).
[3] R. R. A. Syms, E. M. Yeatman, V. M. Bright, and G. M. Whitesides, "Surface tension-powered self-assembly of micro structures—The state-of-the-art," J. Micromech. Microeng. **12**, 387 (2003).
[4] P. K. Maini, K. J. Painter, and H. N. P. Chau, "Spatial pattern formation in chemical and biological systems," J. Chem. Soc., Faraday Trans. **93**, 3601 (1997).
[5] R. Kapral, "Pattern-formation in chemical-systems," Physica D **86**, 149 (1995).
[6] B. A. Grzybowski, A. Winkleman, J. A. Wiles, Y. Brumer, and G. M. Whitesides, "Electrostatic self-assembly of macroscopic crystals using contact electrification," Nat. Mater. **2**, 241 (2003).
[7] N. Bowden, A. Terfort, J. Carbeck, and G. M. Whitesides, "Self-assembly of mesoscale objects into ordered two-dimensional arrays," Science **276**, 233 (1997).

[8]H-J. J. Yeh and J. S. Smith, "Fluidic self-assembly for the integration of GaAs light-emitting-diodes on Si substrates," IEEE Photonics Technol. Lett. **6**, 706 (1994).
[9]J. C. Shelley and M. Y. Shelley, "Computer simulation of surfactant solutions," Curr. Opin. Colloid Interface Sci. **5**, 101 (2000).
[10]S. Anders, S. Sun, C. B. Murray, C. T. Rettner, M. E. Best, T. Thomson, M. Albrecht, J.-U. Thiele, E. E. Fullerton, and B. D. Terris, "Lithography and self-assembly for nanometer scale magnetism," Microelectron. Eng. **61-62**, 569 (2002).
[11]T. L. Breen, J. Tien, S. R. J. Oliver, T. Hadzic, and G. M. Whitesides, "Design and self-assembly of open, regular, 3D mesostructures," Science **284**, 948 (1999).
[12]B. M. Berkovsky, *Proceedings of the International Advanced Course and Workshop on Thermomechanics of Magnetic Fluids*, edited by B. Berkovsky (Hemisphere, Washington, DC, 1978), p. 149
[13]Q. Chen and Z. J. Zhang, "Size-dependent superparamagnetic properties of MgFe2O4 spinel ferrite nanocrystallites," Appl. Phys. Lett. **73**, 3156 (1998).
[14]V. E. Fertman, *Magnetic Fluids Handbook: Properties and Application* (Hemisphere, New York, 1988).
[15]R. E. Rosensweig, *Ferrohydrodynamics* (Dover, Mineola, NY, 1997).
[16]S. Odenbach, "Ferrofluids—magnetically controlled suspensions," Colloids Surf., A **217**, 171 (2003).
[17]R. E. Goldstein, D. P. Jackson, and S. A. Langer, "Dynamics of pattern-formation in magnetic fluids," J. Magn. Magn. Mater. **122**, 267 (1993).
[18]I. J. Jang, H. E. Horng, Y. C. Chiou, C.-Y. Hong, J. M. Yu, and H. C. Yang, "Pattern formation in microdrops of magnetic fluids," J. Magn. Magn. Mater. **201**, 317 (1999).
[19]B. Yellen, G. Friedman, and A. Feinerman, "Printing superparamagnetic colloidal particle arrays on patterned magnetic film," J. Appl. Phys. **93**, 7331 (2003).
[20]A. G. Boudouvis and L. E. Scriven, "Sensitivity analysis of hysteresis in deformation of ferrofluid drops," J. Magn. Magn. Mater. **122**, 254 (1993).
[21]A. Sinha, R. Ganguly, and I. K. Puri, "Magnetically assembled 3-d mesoscopic patterns using a suspension of superparamagnetic nanoparticles," ASME Integrated Nanosystems—Design, Synthesis and Applications, Pasadena, CA, September 2004, Paper No. NANO2004-46091.
[22]H. Hartshorne, C. J. Backhouse, and W. E. Lee, "Ferrofluid-based microchip pump and valve," Sens. Actuators B **99**, 592 (2004).
[23]A. S. Lubbe, C. Bergemann, J. Brock, and D. G. McClure, "Physiological aspects in magnetic drug-targeting," J. Magn. Magn. Mater. **194**, 149 (1999).
[24]P. A. Voltairas, D. I. Fotiadis, and L. K. Michalis, "Hydrodynamics of magnetic drug targeting," J. Biomech. **35**, 813 (2002).
[25]R. Ganguly, S. Sen, and I. K. Puri, "Heat transfer augmentation using a magnetic fluid under the influence of a line-dipole," J. Magn. Magn. Mater. **271**, 63 (2004).
[26]R. Ganguly, S. Sen, and I. K. Puri, "Thermomagnetic convection in a square enclosure using a line dipole," Phys. Fluids **16**, 2228 (2004).
[27]A. Lange, "Kelvin force in a layer of magnetic fluid," J. Magn. Magn. Mater. **241**, 327 (2002).
[28]G. A. van Ewijk, G. J. Vroege, and A. P. Phillipse, "Susceptibility measurements on a fractionated aggregate-free ferrofluid," J. Phys.: Condens. Matter **14**, 4915 (2002).
[29]M. I. Shliomis and V. I. Stepanov, "Rotational viscosity of magnetic fluids—contribution of the Brownian and Neel relaxational processes," J. Magn. Magn. Mater. **122**, 196 (1993).
[30]H. W. Müller and A. Engel, "Dissipation in ferrofluids: Mesoscopic versus hydrodynamic theory," Phys. Rev. E **60**, 7001 (1999).
[31]D. J. Griffiths, *Introduction to Electrodynamics*, 3rd ed. (Prentice-Hall, New Delhi, 2002) (reprint).
[32]M. Zahn, *Electromagnetic Field Theory* (Wiley, New York, 1979). Equation (9) (p. 369) for zero-free current (i.e., $J_f=0$) implies that $\mathfrak{I}_i = \mu_0 M_j \cdot (\partial H_i/\partial xj) + \frac{1}{2}\mu_0 \partial/\partial x_i (M_j M_j)$. Using Maxwell's equation for $J_f=0$, i.e., $\partial H_i/\partial xj = \partial H_j/\partial x_i$, one gets, $\mathfrak{I}_i = M_j(\mu_0 \partial H_j/\partial x_i + \mu_0 \partial M_j/\partial x_i) = M_j \partial B_j/\partial x_i$. However, the body force around a single particle is computed from the volume integral $f_i = \int_v \mathfrak{I}_i DV$, where the particle of volume V is surrounded by the carrier fluid having zero magnetization and Eq. (12) (p. 370) leads to the expression of the force on a single particle as $f_i = \mu_0 m^p{}_j \partial H_i/\partial x_j$.
[33]R. F. Probestein, *Physicochemical Hydrodynamics* (Wiley, New York, 1994).
[34]C. W. Hirt, B. D. Nicols, and N. C. Romero, "SOLA—a numerical algorithm for transient fluid flows," Los Alamos Scientific Laboratory Report No. LA-5852, Los Alamos, NM, 1975.
[35]S. V. Patankar, *Numerical Heat Transfer and Fluid Flow* (Hemisphere, Washington, DC, 1980).
[36]J. J. Becker, F. E. Luborsky, and D. L. Martin, "Permanent magnet materials," IEEE Trans. Magn. **4** (2), 84 (1968).
[37]E. Blūms, J. Plavinš, and A. Chukhrov, "High-gradient magnetic separation of magnetic colloids and suspensions," J. Magn. Magn. Mater. **39**, 147 (1983).
[38]D. Kim and H. Choi, "Laminar flow past a hemisphere," Phys. Fluids **15**, 2457 (2003).